

Synthesis, crystal structure, physical properties and Raman spectroscopy of transition metal phospho-silicides MSi_xP_y ($M = \text{Fe, Co, Ru, Rh, Pd, Os, Ir, Pt}$)

Ch. Perrier, J. Kreisel, H. Vincent*, O. Chaix-Pluchery, R. Madar

Laboratoire de Matériaux et du Génie Physique (UMR 5628 CNRS), Ecole Nationale Supérieure de Physique de Grenoble,
38402 Saint Martin d'Hères, France

Abstract

Single crystals of new materials with general formula MSi_xP_y with $M = \text{Fe, Co, Ru, Rh, Pd, Os, Ir, Pt}$ and $x + y \geq 4$ have been obtained by solution growth from molten tin or by chemical transport reaction using iodine as the transport agent. Physical measurements show they have a semiconducting behaviour with a narrow gap between 0.1 and 0.4 eV at room temperature, a diamagnetic behaviour at room temperature and a paramagnetic behaviour at lower temperature. The crystal structures were determined using X-ray and neutron diffraction. All compounds have low symmetry, monoclinic or triclinic; the Cobalt compound is merohedrally twinned. The M atoms are octahedrally coordinated by the Si and P atoms; Si and P atoms have tetrahedral surroundings. Moreover, they are usually found completely ordered on their respective sites. All these compounds crystallize in non-centrosymmetric space groups. This unusual character has been confirmed by infrared and Raman spectroscopy analysis. Therefore, these materials are potentially interesting for non-linear infrared optic applications.
© 1997 Elsevier Science S.A.

Keywords: Metal silicide; Metal phosphide; Intermetallic crystal structure; Magnetic semiconductor; Intermetallic Raman spectroscopy

1. Introduction

Many binary metal silicides and phosphides were prepared and investigated many years ago [1]. Phosphorus is generally used as a dopant in Si-based IC technology. Since transition metal silicides are now widely used as contacts in VLSI technology, it is of great interest to get a better knowledge of the ternary phases which may result from the interaction of these compounds with a phosphorus-doped silicon. Few ternary systems of silicon-phosphorus-transition metals have been studied. Folberth et al. [2] prepared and

studied CuSi_2P_3 which is isostructural with ordered chalcopyrite. Vogel et al. [3] studied the iron-phosphorus-silicon phase diagram and quoted the existence of the FeSi_4P_4 compound. Il'Nitskaya et al. [4] studied the Ni-Si-P system and determined the crystal structure of $\text{Ni}_{1.68}\text{Si}_{0.88}\text{P}_3$ and NiSi_3P_4 [5,6]. No other phases containing transition metals were reported when we decided to synthesize and characterize such ternary compounds. We have already reported the synthesis, crystal structure and some physical properties of new metal phospho-silicides MSi_xP_y with $M = \text{Fe, Co, Ni, Ru, Rh, Pd, Os, Ir, Pt}$ [7,8]. A detailed study, including in some Raman Spectroscopy cases, of compounds MSi_4P_4 ($M = \text{Fe, Ru, Os}$) [9] and MSi_3P_3 ($M = \text{Rh, Ir, Co}$) [10–12] has been

* Corresponding author.

published. Crystal structures of two platinum compounds PtSi_3P_2 and PtSi_2P_2 are going to be published [13]. Recently, Jeitschko and collaborators began a systematic study of the same ternary phospho-silicides: an ordered sphalerite-like structure has been proposed for NiSi_3P_3 [14]. In this paper we present a general review of members of this transition metal phospho-silicide family rich in non-metallic atoms. New representations of crystal structures using occupied polyhedra are proposed here.

2. Experimental

The crystals, up to 5 mm, were synthesized by the flux technique using tin as the solvent, and the chemical composition was checked by microprobe analysis. The powder samples were prepared from metal elements in evacuated silica tubes. Preparation conditions were previously related [8]. The crystal data and structures were determined from single crystal fragments using a four-circle diffractometer, according to the general process given in Table 1. The atom type (Si or P) occupying the non-metal sites has been found by refining the atomic population on each site. At first, only one isotropic thermal parameter was applied and refined on the non-metal sites. Nevertheless in the case of strong absorption, results for the population of these sites have to be considered cautiously because they are correlated with the absorption corrections. After refinement the final R-factors are of approximately 0.04 for all crystal structures.

Table 1
Data collection and refinement process

Crystal size (mm)	Prismatic fragment, approximately $0.2 \times 0.2 \times 0.2$
Color	Shiny black
Radiation	$\text{MoK}\alpha$ ($\lambda = 0.71073$) Graphite monochromated
Scan mode	ω
Scan width ($^\circ$)	1.40
Measured range	Half the Ewald Sphere, $3^\circ \leq 2\theta \leq 80^\circ$
Period of intensity control	100 reflections
Measured reflections	~ 5000
Absorption correction	Ψ scan or DIFABS
Structure determination [15,16]	Patterson method, or Direct method
Refinement [16]	SHELXL-93 or SHELX-76
Reflections/refined parameters ratio	$\sim 20-50$
Weighting scheme	$w^{-1}(\text{F}^2) = \sigma^2(\text{F}^2) + (0.035\text{F}^2)^2$ or $w^{-1}(\text{F}) = \sigma^2(\text{F}) + 0.02\text{F}^2$
Agreement factors	$\sim R = 0.04$ on F $\sim \text{WR}_2 = 0.10$ on F^2

The electric resistivity and magnetization measurements were performed between 2 and 300 K on crystals or ceramics using either a Van der Pauw device or a Foner magnetometer [11,12]. The Raman spectra were collected using a Dilor XY multichannel spectrometer, equipped with a microscope [10,11].

3. Crystal data and structures

Table 2 gives the cell and the space group of the all prepared phospho-silicides. All compounds have low symmetry, monoclinic or triclinic; the cobalt compound, apparently orthorhombic is in fact monoclinic and merohedrally twinned. All these compounds crystallize in non-centrosymmetric space groups. This unusual character inferred by the statistical Wilson analysis has been confirmed by non-linear optical tests and infrared and Raman spectroscopy studies. In all the compounds, the metal atoms are always octahedrally surrounded by silicon and phosphorus atoms, and all non-metal atoms are tetrahedrally coordinated by metal or non-metal atoms; so one observes tetrahedra with zero, one, two or three metal atoms at the vertices. In fact, tetrahedra with M atoms at vertices are not occupied independent polyhedra. These tetrahedra overlap with octahedra, while one, two or three of their corners are located at the center of one, two or three octahedra. The differences in the atomic arrangements of these compounds are reflected in the different way in which the $\text{M}(\text{Si}/\text{P})_6$ octahedra are separated or linked via common corners or /and edges. The structure of NiSi_3P_3 is different. According to Il'Nitskaya [5], the structure which is non-centrosymmetric can also be described as an arrangement of only tetrahedra where Ni and Si atoms are surrounded by P atoms and P atoms by Ni and Si atoms.

3.1. RhSi_3P_3 and IrSi_3P_3

Both compounds are isostructural. The structure pattern is constituted by one $\text{M}(\text{Si}_3\text{P}_3)_6$ octahedron. Two Si atoms occupy two opposite vertices, one Si and three P atoms, randomly distributed, occupy the four other vertices. Each octahedron, slightly elongated along the Si-Si direction, is alone without sharing any common corner with another one (Fig. 1). Neglecting the off-mirror position of the Si site, the crystal structure could be viewed as centric. The structure could even be described in the Cm space group, in this case Si and P atoms could be located on their own sites without mixing. Nevertheless statistical examination of equivalent reflections shows clearly that the point-group symmetry is P2, furthermore the structural refinement in C2 gave the best results for

Table 2
Cell parameters, space group and cell content

Formula	Cell parameters (Å and °)	S.G	Z
RhSi ₃ P ₃	$a = 6.626(1), b = 7.210(1), c = 5.522(1), \beta = 118.31(1)$	C2	2
IrSi ₃ P ₃	$a = 6.577(2), b = 7.229(2), c = 5.484(2), \beta = 117.91(1)$	C2	2
FeSi ₄ P ₄	$a = 4.876(1), b = 5.545(1), c = 6.064(1), \alpha = 85.33(3), \beta = 68.40(4), \gamma = 70.43(2)$	P1	1
RuSi ₄ P ₄	$a = 4.936(1), b = 5.634(1), c = 6.162(1), \alpha = 85.51(1), \beta = 68.26(1), \gamma = 70.69(1)$	P1	1
OsSi ₄ P ₄	$a = 4.948(1), b = 5.620(1), c = 6.175(1), \alpha = 85.65(3), \beta = 68.36(1), \gamma = 70.89(1)$	P1	1
CoSi ₃ P ₃	$a = 5.899(1), b = 5.703(1), c = 12.736(2), \beta = 90.00(1)$	P2 ₁	4
PtSi ₃ P ₂	$a = 4.840(1), b = 5.482(1), c = 8.052(2), \alpha = 91.57(1), \beta = 93.52(1), \gamma = 108.14(1)$	P1	2
PtSi ₂ P ₂	$a = 6.025(1), b = 9.468(1), c = 11.913(1), \beta = 102.91(1)$	P2 ₁	8

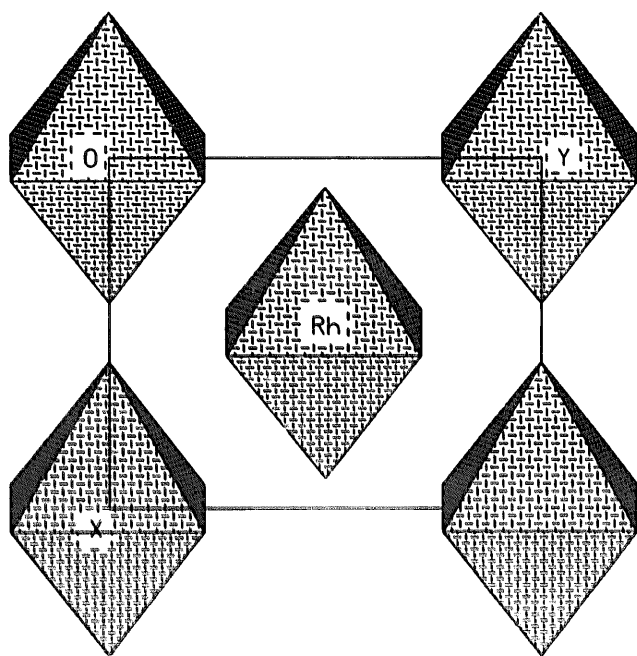


Fig. 1. MSi₃P₃ crystal structure viewed along the c-axis.

the two phospho-silicides. Results obtained by Raman spectroscopy are in complete agreement with this conclusion [9,10].

3.2. FeSi₄P₄, RuSi₄P₄ and OsSi₄P₄

These three compounds are isostructural. The structure pattern is made up by one octahedron M(Si₃P₃) and two completely non-metallic overlapped tetrahedra having a same axis; one Si(P₄) tetrahedron with four P corners overlaps one P(Si₄) tetrahedron with four Si corners. In fact this atomic arrangement can be viewed as a pair of Si–P atoms located in a large octahedron of three Si and three P vertices. This large Si–P pair octahedron shares one corner with six M octahedra and takes part in the structure cohesion. Each octahedron is isolated with no common corner with another one (Fig. 2) [8].

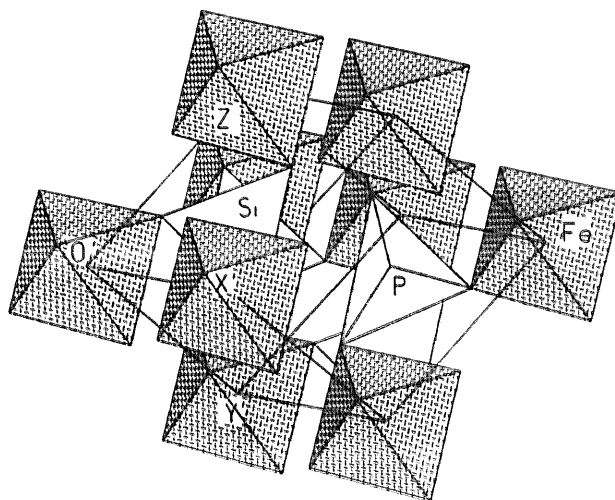


Fig. 2. MSi₄P₄ crystal structure viewed along the [0-11] direction.

3.3. CoSi₃P₃

The lattice of CoSi₃P₃ is orthorhombic and an average crystal structure of this compound can be described in the orthorhombic space group P2₁2₁2₁ with a mediocre agreement factor ($R = 0.067$). In fact, all crystals are merohedrally twinned. The true symmetry is monoclinic and the true space group is P2₁ ($R = 0.035$). The structure pattern is constituted by two Co(Si₃P₃) octahedra and two non-metallic tetrahedra Si(P₄) and P(Si₄). Contrary to the previous structures in which the metal octahedra are isolated, each Co octahedron is linked by two Si corners to two Co octahedra forming an infinite zigzag chain along the b-axis direction. In the same way, Si tetrahedra linked by P vertices and P tetrahedra linked by Si vertices form two infinite zigzag chains along the same direction. None of the chains have a common corner and stand apart from each other. The separate Co octahedra chains are connected to each other by P and Si tetrahedra chains (Fig. 3) [11].

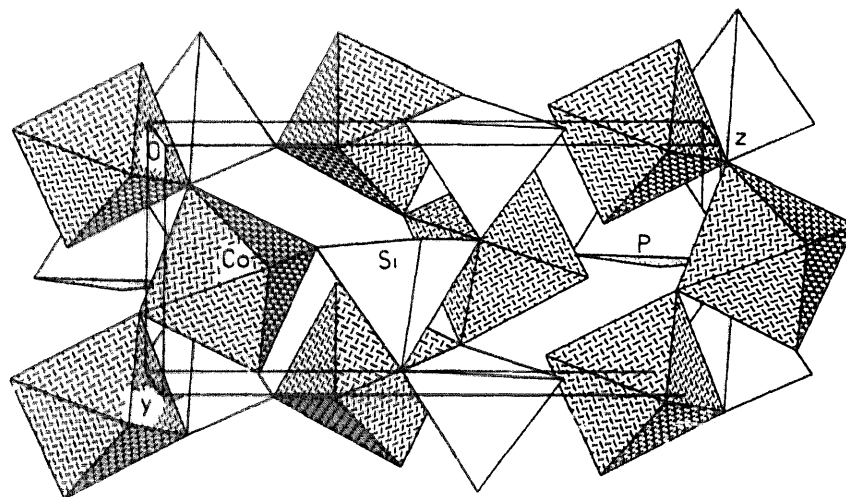


Fig. 3. CoSi_3P_3 crystal structure viewed along the *a*-axis.

3.4. PtSi_3P_2 and PtSi_2P_3

The PtSi_3P_2 structure can be described by two crystallographically independent Pt octahedra connected pairwise by edge-sharing. The resulting $\text{Pt}_2(\text{Si}/\text{P})_{10}$ double-octahedron constitutes the crystal structure pattern. On both sides of the Si–Si common edge, each Pt atom is surrounded by two phosphorus and two silicon atoms. In principle, metal–metal bonding could occur when octahedra are paired with one common edge like in MnP_3 . Here, the distortions of Pt octahedra are such that in a double octahedron, the metal atoms remain widely separate ($\text{Pt}–\text{Pt} = 3.77 \text{ \AA}$). Two neighbouring double-octahedra have no common corner, they are linked to each other only by

bonds between non-metal atoms ($–\text{Si}/\text{P}–\text{Si}/\text{P}–$) (Fig. 4).

The PtSi_2P_3 crystal structure pattern can be described by a cluster of four edge-sharing $\text{Pt}(\text{Si}_3\text{P}_3)$ octahedra and by two non-metallic $\text{P}(\text{SiP}_3)$ and $\text{Si}(\text{PSi}_3)$ tetrahedra. No metal–metal bonding occurs (shortest $\text{Pt}–\text{Pt} = 3.70 \text{ \AA}$). Moreover, while octahedral couples are separated from each other in the PtSi_3P_2 structure, two neighbouring clusters are linked by one common corner and the completely non-metallic tetrahedra P and Si establish bonding between four clusters (Fig. 5) [12].

4. Raman spectroscopy

We decided to analyze and characterize MeSi_3P_3

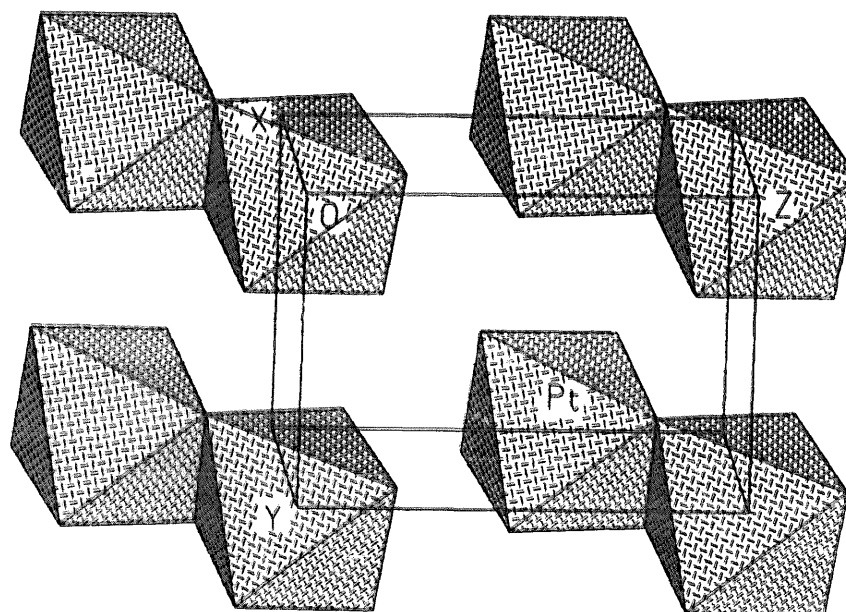


Fig. 4. PtSi_3P_2 crystal structure viewed along the *a*-axis.

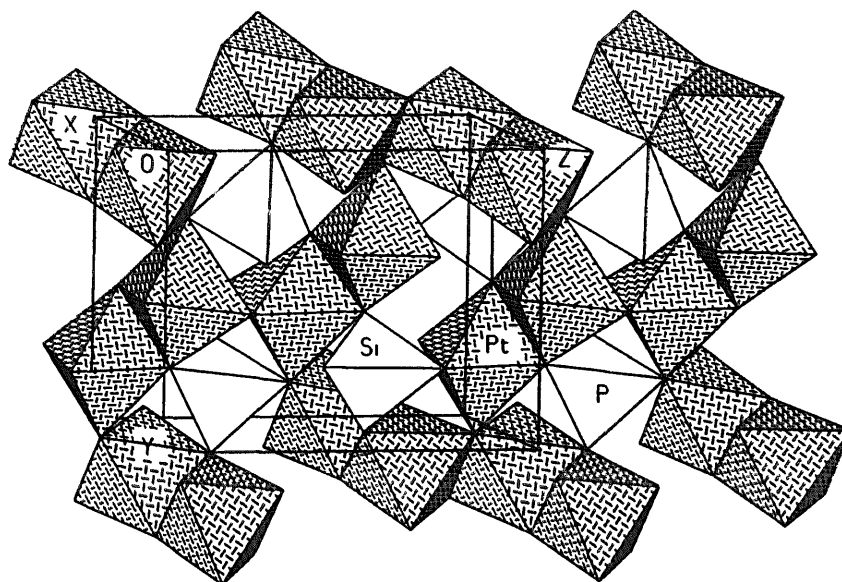
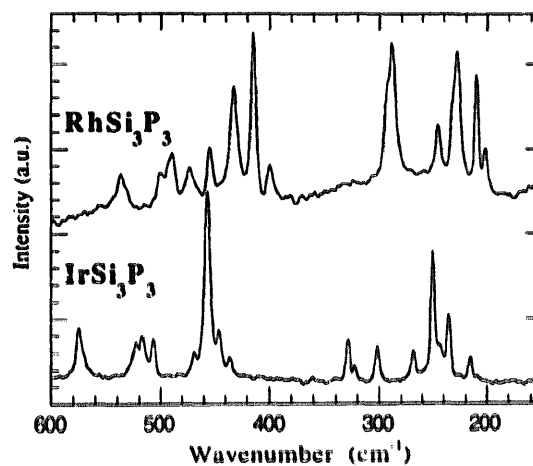
Fig. 5. PtSi_2P_2 crystal structure viewed along the a-axis.

Table 3
Raman active modes of some phospho-silicides. A full calculation of the irreducible representations is given [10,11,13]

	Raman active modes	
	Centred	Non-centred
MeSi_3P_3 (Ir, Rh)	5 Ag + 4 Bg	9 A + 9 B
MeSi_4P_4 (Fe, Ru, Os)	12 Ag	24 A

(Me = Fe, Co, Ru, Rh, Os, Ir) [10,11,13] by Raman spectroscopy to get a better knowledge of their structural and physical properties. Furthermore, in view of the in-situ Raman control of silicide films obtained during CVD process [17], the present results contribute to collect a data bank on the silicon compounds.

Since the centrosymmetry in the phospho-silicides cannot be completely ascertained by diffraction methods, we have calculated the total irreducible representation to interpret the experimental Raman spectra. Some selected results are presented in Table 3 and show that Raman spectroscopy should be an excellent technique to distinguish between centred and non-centred structures. The observed Raman spectra obtained from single crystals and powders, show that all the tested phospho-silicides crystallize unambiguously in a non-centred structure. These conclusions are obtained by simple comparison between the number of calculated and observed lines. Representative single crystal spectra are shown in Fig. 6. A more detailed analysis of RhSi_3P_3 and IrSi_3P_3 , by using normal mode calculations has been presented in Kreisel et al. [10].

Fig. 6. Raman spectra of RhSi_3P_3 and IrSi_3P_3 .

Raman spectroscopy has also been used to analyse the crystal structure of CoSi_3P_3 discussed above. In order to check the actual crystal symmetry (orthorhombic or monoclinic) the irreducible representation has been calculated and band assignment has been performed for both P2_1 and $\text{P2}_12_12_1$ (C_2^2 and D_2^4) possible space groups [11]. The 28 atoms of the primitive cell give rise to 81 zone centre vibrational modes. In the C_2^2 space group, all (41A + 40B) modes are Raman- and IR-active. In the D_2^4 space group, 60 (20B₁ + 20B₂ + 20B₃) modes are Raman- and IR-active and 21 A modes are Raman-active. In order to distinguish between the two proposed models, several polarisation configurations have to be used. In the experimental spectra 31 bands are observed in the $\text{Z}(\text{XX})\bar{\text{Z}}$ configuration instead of the expected 41 in the monoclinic- or 21 in the orthorhombic structure. The absence of some lines (too weak or masked by

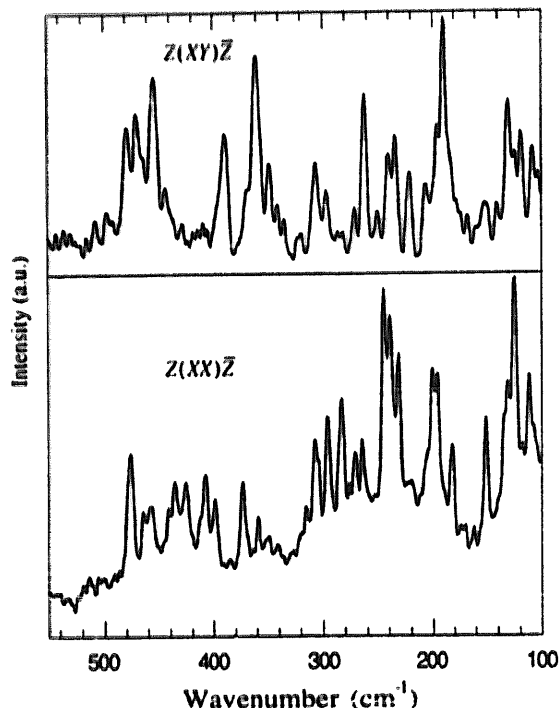


Fig. 7. Polarized Raman spectra of CoSi_3P_3 .

stronger lines of the same mode) is compatible with the monoclinic case but a large excess of bands is not acceptable; thus, the orthorhombic structure must be ruled out. This conclusion is strengthened by the observation of 32 bands in the $Z(XY)\bar{Z}$ configuration instead of 40 in the monoclinic assumption or 20 in the orthorhombic one (Fig. 7). The observed frequencies and band assignment are given in Vincent et al. [11].

5. Physical characterization

5.1. Electrical resistivity

The electric resistivity of most of the phospho-silicides has been measured using single crystals and ceramics between 300 and 80 K. Ceramic discs were prepared by powder sintering at 700 K for 1 week in evacuated silica tubes. Van der Pauw's method was used for measurements of both kinds of sample. Observed energy gaps are similar, only the initial resistivity values are different because of the resistivity of grain boundaries in the ceramics. The obtained results on crystals and ceramics are summarized in Table 4.

Most of the phospho-silicides are semiconducting. As seen in Fig. 8, FeSi_4P_4 is semiconducting with 0.3 $\Omega\text{ cm}$ resistivity and a small gap energy, $E_g = 0.15\text{ eV}$ at room temperature. Because of the presence of some impurity band as suggested by the low temperature magnetic susceptibility, apparent E_g decreases

Table 4

Electrical properties of some phospho-silicides observed at room temperature

		Resistivity (Ωcm)	Gap (eV)
CoSi_3Si_3	Crystal	0.62	0.12
	Ceramic	90	0.15
FeSi_4P_4	Crystal	0.3	0.15–0.20
	Ceramic	322	0.27
RuSi_4P_4	Ceramic		0.25
$\text{NiSi}_{3.25}\text{P}_{4.3}$	Ceramic		0.11
PtSi_3P_2	Crystal	Slight metallic behaviour	
RhSi_3P_3	Crystal	Slight metallic behaviour	

with the temperature, $E_g = 0.029\text{ eV}$ at 80 K. Fairly similar behaviour has been observed for CoSi_3P_3 [11].

Fig. 9 presents the resistivity of a RhSi_3P_3 single crystal between 4.2 and 300 K. In nearly the whole temperature range the resistivity increases with temperature but this variation is quite small, only approximately 20%. The curve exhibits two regimes: above 50 K, ρ increases linearly with T and below this temperature follows a somewhat higher power law. It is, however, not possible to ascribe this behaviour to a metallic one, as the absolute resistivity values are quite high (some $\text{m}\Omega\text{ cm}$), and at lowest temperature no constant residual resistivity can be observed in a significant temperature range, as expected for a metal. Phospho-silicides which have not been investigated are very hygroscopic: it was impossible to measure the resistivity by the four contacts method. More detailed investigations are necessary to classify the electrical behaviour of these materials unambiguously.

5.2. Magnetic susceptibility

Magnetization measurements on powder have been performed, between 10 and 300 K using a Foner

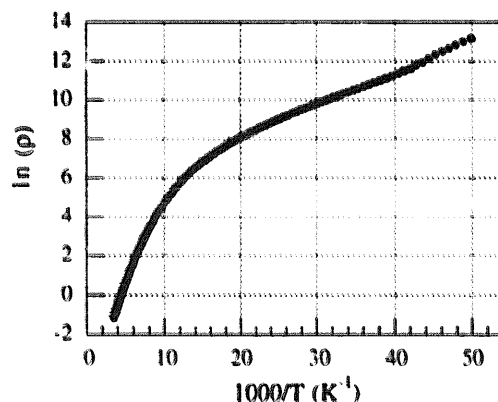


Fig. 8. FeSi_4P_4 resistivity measured on single crystal.

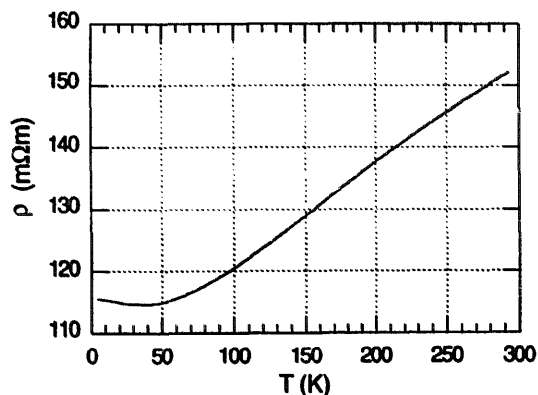


Fig. 9. RhSi_3P_3 resistivity measured on single crystal.

magnetometer and between 300 and 1200 K using the Faraday method. All the tested phospho-silicides are paramagnetic at low temperature (transition temperature at 15–65 K, depending on the transition metal) and diamagnetic above. Fig. 10 shows $\chi(T)$ for IrSi_3P_3 after correction of the sample holder contribution.

The magnetic susceptibility of a semiconductor is mainly the sum of the lattice and charge carrier susceptibilities: $\chi = \chi_l + \chi_c$. The χ_l term results from diamagnetism of the core electrons; its value is temperature independent and can be calculated from tabulated values for different ions [18]. The term χ_c is either a contribution of Pauli's paramagnetism or a contribution of classical paramagnetism resulting from a magnetic impurity band of carriers localized at low temperature in an isolating state near the conduction band. Assuming the electronic core configuration of each element is the same as in transition metal silicides i.e. Me^+ and Si^{2+} [19] and assuming the phosphorus one is P^{5+} , the lattice susceptibility can be calculated. A comparison between the observed and calculated susceptibility is given in Fig. 11. The overall agreement is very good, which confirms the experi-

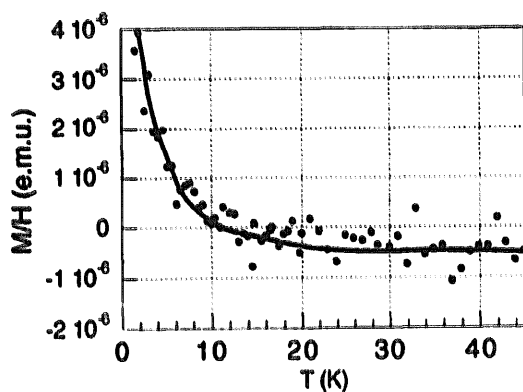


Fig. 10. IrSi_3P_3 magnetic susceptibility vs. T .

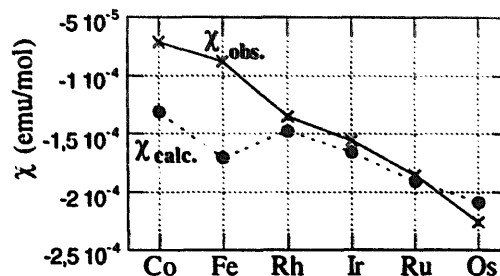


Fig. 11. Observed and calculated susceptibility at 500 K for MeSi_xP_y .

ment and indicates a dominating diamagnetism at high temperature. The discrepancies observed for 3d transition metals (Co, Fe), is due to a classical paramagnetic contribution χ_c . The absence of data needed for a detailed calculation of band structure makes it difficult to describe this behaviour more precisely.

References

- [1] B. Aronson, T. Lundström, S. Rundqvist, Borides, Silicides and Phosphides, Methuen, London, 1965.
- [2] O.G. Folberth, H. Pfister, Acta Cryst. 14 (1961) 325.
- [3] R. Vogel, B. Giessen, Arch. Eisenhüttenw 30 (1959) 619.
- [4] O.N. Il'Nitskaya, Yu.B. Kuz'ma, Zh. Neorg. Khim. 37 (1992) 729.
- [5] O.N. Il'Nitskaya, V.A. Bruskov, P.Yu. Zavalii, Yu.B. Kuz'ma, Izv. Akad. Nauk SSSR, Neorg. Mater. 27 (1991) 1311.
- [6] H. Vincent, Ch. Perrier, M. Kirschen, P. Chaudouet, R. Madar, 11th ICSCTE, Wrocław, 1994.
- [7] Ch. Perrier, Thesis, Institut National Polytechnique de Grenoble, 1995.
- [8] Ch. Perrier, H. Vincent, P. Chaudouet, B. Chenevier, R. Madar, Mat. Res. Bull. 30 (1995) 357.
- [9] M. Kirschen, H. Vincent, Ch. Perrier, P. Chaudouet, B. Chenevier, R. Madar, Mat. Res. Bull. 30 (1995) 507.
- [10] J. Kreisel, O. Chaix-Pluchery, F. Genet, G. Lucazeau, H. Vincent, R. Madar, J. Solid State Chem. 128 (1997) 142.
- [11] H. Vincent, J. Kreisel, Ch. Perrier, O. Chaix-Pluchery, P. Chaudouët, R. Madar, J. Solid State Chem. 124 (1996) 366.
- [12] Ch. Perrier, J. Kreisel, O. Chaix-Pluchery, G. Lucazeau, H. Vincent, R. Madar, J. Solid State Chem., submitted.
- [13] Ch. Perrier, M. Kirschen, H. Vincent, U. Gottlieb, B. Chenevier, R. Madar, J. Solid State Chem., accepted.
- [14] J. Wallinda, W. Jeitschko, J. Solid State Chem. 114 (1995) 476.
- [15] Structure Determination Package, B.A. Frenze, College Station, Texas 77840, 1985.
- [16] SHELX93, G. Sheldrick, Institut Anorg. Chemie, D-37077 Göttingen, 1993.
- [17] L. Fayette, B. Marcus, M. Mermoux, N. Rosman, L. Abello, G. Lucazeau, J. Appl. Phys. 76 (1994) 1604.
- [18] E. König, G. König, in: K.H. Hellwege (Ed.), Magnetic Properties of Coordination and Organometallic Transition Metal Compounds, Landolt-Börnstein, vol. II, part 10., Springer, Berlin, 1979.
- [19] U. Gottlieb, A. Sulpice, R. Madar, O. Laborde, J. Phys. Condens. Matter 5 (1993) 8755.